WDM-based optical wireless communication using Panda ring resonators

ALI SHAHIDINEJAD*
Department of Computer Engineering, Qom branch, Islamic Azad University, Qom, Iran

In this paper, a system of Panda ring resonator and a wavelength router are proposed to generate localized multi wavelength, applicable for WDM-based optical wireless communication (OWC). When a Gaussian beam is introduced into the proposed Panda system, highly chaotic signals are generated because of the nonlinear Kerr effect. Then the proposed wavelength router in the system filters the chaotic signals and specific wavelengths of λ_0 = 1550.51 nm, λ_1 = 1551.19 nm, λ_2 = 1551.87 nm and λ_3 = 1552.55 nm are generated. The performance of the proposed system is analysed in terms of Q-factor and bit error rate (BER). During the analysis, the proposed pulse shape is compared against the conventional rectangular and Gaussian methods. Results show the superiority of the proposed system for WDM-based OWC.

(Received November 23, 2017; accepted August 9, 2018)

Keywords: Optical wireless communication, Wavelength, Panda ring resonator, BER, Q-factor

1. Introduction

Optical wireless communication (OWC) can be an interesting alternative to RF and fibre optic communication systems, because of license-free operation, immunity to electromagnetic interference, ease of deployment, low power consumption, high security [1]. Outdoor WDM-based OWC is generally used in order to bridge two different networks. WDM technique can be easily integrated with the outdoor OWC systems and it is able to considerably increase the bitrate of them.

Outdoor WDM-based OWC system was first proposed by Song et al. [2]. They presented 40 Gb/s data transmission over 1.2 km using four different wavelengths. After that, Jeong et al. [3] applied more wavelengths (eight wavelengths) and they reached 80 Gb/s and Chen et al. [4] proposed a 160 Gb/s data transmission over 2.16 km using 16 different wavelengths. A new full OWC terminal was introduced by Matsumoto et al. [5], in which the OWC transmitter/receiver is directly connected to the optical fibre, which leads to a higher speed and lower BER. Following the previous method, the concept of advanced WDM radio over free space was demonstrated by Tsukamoto et al. [6], high data transmission of 320 Gbit/s over 210 m by Arimoto et al. [7], and 1.28 Terabit/s by Ciaramella et al. [8] were realized. Original measurement results from an all-optical 10 Gbit/s FSO relay link involving two FSO links and an all-optical switch was presented by [9]. Following the previous method, the idea of progressive WDM radio over FSO was demonstrated by [6, 10]. The German Aerospace Center (DLR) and the European Southern Observatory performed a measurement campaign together in April and July 2016 at Teide-Observatory, with the support of the European Space Agency, to investigate the use of laser guide stars in ground to space optical communications [11]. In fact, WDM-based OWC could reach higher data transmission rates than previously expected and became an interesting alternative for a much wider range of outdoor usages [12].

The availability of the proposed systems in [2-5] is less than a minute. The introduced systems in [7, 8] demonstrate a better availability and reliability compared to other works, however reliability and capacity (compared to optical fibre capacity) are still two main challenges in outdoor systems [13]. Different techniques have been proposed to compensate for the mentioned problems by using receivers with large receive apertures [14], using enhanced modulation techniques [15, 16], multi-input multi-output configuration [17] and the use of different pulse shapes for transmission [18]. Following the last technique, this research tries to enhance WDM-based OWC function by proposing solitonic pulse shape and generating accurate wavelengths using micro ring resonators (MRRs). Optical soliton is known as a nonlinear solitary wave. After that it has been broadly studied in different areas for instance in mathematics, physics and recently optical communication systems. The most interesting features of a solitonic pulse shape are cross phase modulation (CPM) and self-phase modulation (SPM). Moreover, the key advantage of soliton pulse is its non-dispersion behavior. Therefore, it can be utilized in long distance communication, where the long distance communication can be achieved without repeaters.

MRR has many interesting applications because of its own nature and showing an effective performance for generating solitonic mm-wave and micro wave generation [19, 20]. MRR could be an interesting technology to reach a high capacity WDM-based OWC channel with accurate free spectral range (FSR), full width at half maximum (FWHM), and intensity [21]. Panda ring resonator system consists of a centered MRR connected to two smaller rings on the right and left sides [22].

In order to simulate the optical soliton propagating within the microring resonator, MATLAB environments have been used. In this research, an iterative method is applied in order to calculate the output power of each round trip of the input pulse within the ring system. Real data from practical experiments were used for simulating the proposed system. After that, a WDM-based OWC system is simulated and the proposed system is imported to OptiSystem in order to evaluate and compare the proposed method against traditional methods.

2. Theoretical background

MRRs can be integrated in array geometries to implement many useful functions. Its nonlinear phase response can be incorporated into an interferometer to produce specific intensity output function [23]. A schematic of the proposed Panda ring resonator connected to the wavelength router is shown in Fig. 1. This system is used to generate desired wavelengths and pulses applicable for WDM-based OWC. Panda ring resonator system generates highly chaotic signals because of the nonlinear Kerr effect as shown in Fig. 1(a). The router device filters the chaotic signals and generates specific wavelengths of λ_0, λ_1, λ_2 and λ_3, as can be seen in Fig. 1(b).

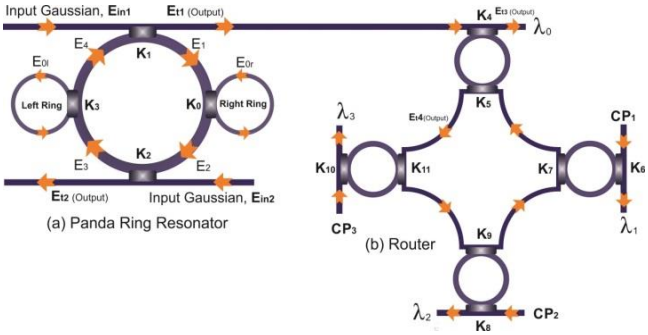

Fig. 1. Proposed micro ring resonator connected to a wavelength router.

An optical Gaussian beam is introduced into the Panda ring resonator which is given by Eq. (1) [24].

$$E_{in1}(t,z) = E_{in2}(t,z) = E_0 \exp\left[\left(\frac{z}{2L_D}\right) - i\omega_0 t\right] \quad (1)$$

The amplitude and propagation distance are defined by E_0 and z. The dispersion length of the pulse is defined by L_D, where ω_0 is the carrier frequency. The Gaussian distribution of the input beam is on the longitudinal direction. The output signals on the right side of the Panda system are given as Eq. (2) and Eq. (3):

$$E_1 = \sqrt{1-\gamma_1}\left(\sqrt{1-\kappa_1}E_4 + j\sqrt{\kappa_1}E_{in1}\right) \quad (2)$$

$$E_2 = E_{0r}E_1 e^{-\frac{\alpha}{2}\frac{L}{2} - jk_n\frac{L}{2}}, \quad (3)$$

where κ_1 is the intensity coupling coefficient. The coupling coefficient of resonators is a dimensionless value that characterizes interaction of two resonators. Coupling coefficients are used in resonator filter theory. Resonators may be both electromagnetic and acoustic. Coupling coefficients together with resonant frequencies and external quality factors of resonators are the generalized parameters of filters. γ_1 is fractional coupler intensity loss and α is attenuation coefficient. $k_n = 2\pi/\lambda$ is the wave propagation number, λ is the input wavelength and $L = 2\pi R_{PANDA}$ where, R_{PANDA} is the radius of the Panda system. E_{0r} is the electric field of the ring on the right side of the Panda rings system which is given by Eq. (4):

$$E_{0r} = E_1 \frac{\sqrt{(1-\gamma)(1-\kappa_0)} - (1-\gamma)e^{-\frac{\alpha}{2}L_1 - jk_nL_1}}{1-\sqrt{1-\gamma}\sqrt{1-\kappa_0}e^{-\frac{\alpha}{2}L_1 - jk_nL_1}}, \quad (4)$$

where $L_1 = 2\pi R_r$, R_r and κ_0 are the radius and coupling coefficient of the right ring respectively. Light fields of the left side of the Panda ring resonator can be expressed as Eq. (5) and Eq. (6):

$$E_3 = \sqrt{1-\gamma_2}\left[\sqrt{1-\kappa_2}E_2 + j\sqrt{\kappa_2}E_{in2}\right], \quad (5)$$

$$E_4 = E_{0L}E_3 e^{-\frac{\alpha}{2}\frac{L}{2} - jk_n\frac{L}{2}}, \quad (6)$$

where,

$$E_{0L} = E_3 \frac{\sqrt{(1-\gamma)(1-\kappa_3)} - (1-\gamma)e^{-\frac{\alpha}{2}L_2 - jk_nL_2}}{1-\sqrt{1-\gamma}\sqrt{1-\kappa_3}e^{-\frac{\alpha}{2}L_2 - jk_nL_2}} \quad (7)$$

Here, $L_2 = 2\pi R_L$ and R_L is the left ring's radius. To simplify these equations, the parameters of x_1, x_2, y_1 and y_2 are defined as: $x_1 = (1-\gamma_1)^{\frac{1}{2}}$, $x_2 = (1-\gamma_2)^{\frac{1}{2}}$, $y_1 = (1-\kappa_1)^{\frac{1}{2}}$, and $y_2 = (1-\kappa_2)^{\frac{1}{2}}$.

Therefore,

$$E_1 = \frac{jx_1\sqrt{\kappa_1}E_{in1} + jx_1x_2y_1\sqrt{\kappa_2}E_{0L}E_{in2}e^{-\frac{\alpha}{2}\frac{L}{2} - jk_n\frac{L}{2}}}{1 - x_1x_2y_1y_2E_{0r}E_{0L}e^{-\frac{\alpha}{2}L - jk_nL}} \quad (8)$$

$$E_3 = x_2y_2E_{0r}E_1 e^{-\frac{\alpha}{2}\frac{L}{2} - jk_n\frac{L}{2}} + jx_2\sqrt{\kappa_2}E_{in2} \quad (9)$$

$$E_4 = x_2 y_2 E_{0r} E_{0L} E_1 e^{-\frac{\alpha}{2}L - jk_n L} + jx_2\sqrt{\kappa_2} E_{0L} E_{in2}\, e^{-\frac{\alpha}{2}\frac{L}{2} - jk_n \frac{L}{2}} \quad (10)$$

As shown in Fig. 1, the electric fields from through and drop ports of the Panda ring resonator are E_{t1} and E_{t2} which can be expressed by following equations [20]:

$$E_{t1} = AE_{in1} - BE_{in2} e^{-\frac{\alpha}{2}\frac{L}{2} - jk_n \frac{L}{2}} \left[\frac{CE_{in1}G^2 + DE_{in2}G^3}{1 - FG^2} \right] \quad (11)$$

$$E_{t2} = x_2 y_2 E_{in2} \left[\frac{A\sqrt{\kappa_1\kappa_2} E_{0r} E_{in1} G + \frac{D}{x_1\sqrt{\kappa_1} E_{0L}} E_{in2} G^2}{1 - FG^2} \right] \quad (12)$$

where,

$A = x_1 x_2$, $B = x_1 x_2 y_2 \sqrt{\kappa_1} E_{0L}$, $C = x_1^2 x_2 \kappa_1 \sqrt{\kappa_2} E_{0r} E_{0L}$, $D = (x_1 x_2)^2 y_1 y_2 \sqrt{\kappa_1\kappa_2} E_{0r} E_{0L}^2$, $G = \left(e^{-\frac{\alpha}{2}\frac{L}{2} - jk_n \frac{L}{2}} \right)$ and $F = x_1 x_2 y_1 y_2 E_{0r} E_{0L}$.

As shown in Fig. 1, electric fields of the add/drop filter system can be expressed by Eq. (13) and Eq. (14) regarding to the inserted E_{t1} as input pulse.

$$|E_{t3}|^2 = |E_{t1}|^2 \times ((1-\kappa_4) - 2\sqrt{1-\kappa_4} \cdot \sqrt{1-\kappa_5} e^{-\frac{\alpha}{2}L} \cos(k_n L) + (1-\kappa_5) e^{-\alpha L}) / (1 + (1-\kappa_4)(1-\kappa_5) e^{-\alpha L} - 2\sqrt{1-\kappa_4} \cdot \sqrt{1-\kappa_5} e^{-\frac{\alpha}{2}L} \cos(k_n L)) \quad (13)$$

$$|E_{t4}|^2 = |E_{t1}|^2 \times \kappa_4 \kappa_5 e^{-\frac{\alpha}{2}L} / (1 + (1-\kappa_4)(1-\kappa_5) e^{-\alpha L} - 2\sqrt{1-\kappa_4} \cdot \sqrt{1-\kappa_5} e^{-\frac{\alpha}{2}L} \cos(k_n L)) \quad (14)$$

where, κ_4 and κ_5 are the coupling coefficients of the add/drop device. As shown in Fig. 1, control ports 1, 2 and 3 (Cp_1, Cp_2 and Cp_3) are the second input for the add/drop devices applied in the wavelength router like E_{in2} for the Panda ring resonator. Control ports are used in order to adjust the output of each add/drop device to a desired wavelength. In order to simulate the wavelength router, the throughput port of each add/drop device is considered as the input of the neighbouring device except for the add/drop device that is connected to the Panda ring resonator.

The performance of the proposed MRR system is evaluated in terms of Q-factor and BER. As can be found from Eq. (15), Q-factor is the difference between the mean values of the signal levels for a "1" and a "0" (μ1 and μ0), divided by the sum of the noise values (σ1 and σ0) at those two signal levels assuming Gaussian noise and the probability of a '1' and '0' transmission being equal (P(1) = P(0) = ½).

$$Q = (\mu 1 - \mu 0) / (\sigma 1 + \sigma 0) \quad (15)$$

3. Results and discussion

The input is considered as a Gaussian beam with power of 1W with centre wavelength of 1550nm, inserted into the Panda ring resonator. The fixed parameters of the proposed system are shown in Table 1, where n_0 is linear refractive index, γ is fractional coupler intensity loss, n_2 is nonlinear refractive index, α is ring resonator loss, A_{effp} is effective core area of the centre ring of the Panda and λ_0 is central wavelength.

Table 1. Parameters of Panda resonator system

Symbol	Value	Symbol	Value
R_{Panda} (μm)	180	K_6	.91
R_r (μm)	7	K_7	.98
R_l (μm)	7	K_8	.93
K_0	.2	K_9	.97
K_1	.35	K_{10}	.95
K_2	.1	K_{11}	.98
K_3	.95	n_0	3.34
K_4	.92	γ	.01
K_5	.96	$n_2\,(m^2W^{-1})$	1.3×10^{-13}

The input Gaussian beam is shown in Fig. 2(a), the signals on the right side of the Panda system are shown in Fig. 2(b-c) and Fig. 2(d-e) shows the signals on the left side of the system. More channel capacity can be obtained and controlled by generating a large bandwidth of chaotic signals. Therefore, stable signals of the chaotic signals can be seen within the through port of the system, which is required to be used as an input power inserted into the proposed wavelength router system as shown in Fig. 2(f). This fact helps the wavelength router to have more options in order to filter the desired wavelengths.

Fig. 3 illustrates the throughput output power of each add/drop devices in the proposed router system. As can be seen in the figure centre wavelengths of λ_0 = 1550.51 nm, λ_1 = 1551.19 nm, λ_2 = 1551.87 nm and λ_3 = 1552.55 nm are obtained.

FWHM for a solitonic pulse shape is considerably narrower than Gaussian and rectangular pulse shapes and decreasing the duty cycle leads to having a lower bit error rate (BER) [18]. However, the pulse width should be larger than 10 ps, because the pulse broadening is very significant when the pulse width is in the order of 2 ps. Outdoor WDM-based OWC systems could have a better performance by using enhanced pulse shapes like solitonic pulse shape. Moreover, in WDM-based OWC studies, one of the most important issues is to achieve a higher capacity

with specific FSR, FWHM and intensity. In all previous studies on outdoor WDM OWC, the generated wavelengths are not exactly separated and there are power fluctuations between different wavelength and these deviations decrease the reliability and are not desired [2-5, 7, 8]. The proposed system offers dense wavelengths with exact and appropriate FSR, FWHM and intensity.

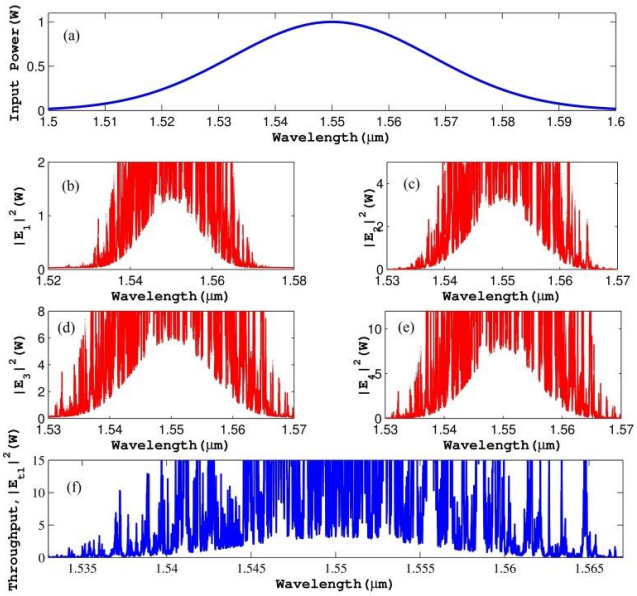

Fig. 2. Chaotic signals generated by the Panda system, where (a): Input Gaussian beam, (b): $|E_1|^2$, (c): $|E_2|^2$, (d): $|E_3|^2$, (e): $|E_4|^2$ and (f): $|E_{t1}|^2$.

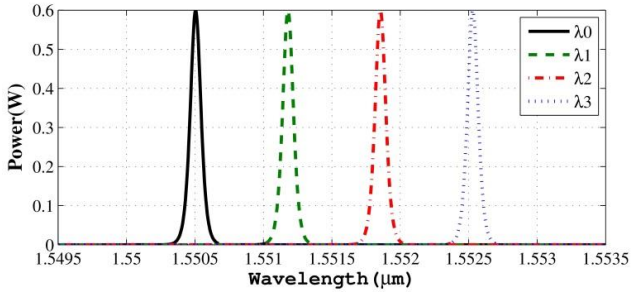

Fig. 3. Throughputs of each add/drop devices in the router system

The schematic of a WDM-based OWC system is shown in Fig. 4. As can be seen in this figure, there is a line of sight between the transmitter and receiver (250 m distance). A number of modulated optical carrier waves are multiplexed onto a single fibre optic. Each optical carrier wave is typically labelled by its wavelength.

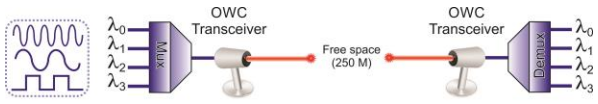

Fig. 4. WDM-based OWC system

A WDM-based OWC system applies a multiplexer at the transmitter part to join together the optical waves with different wavelengths, and a demultiplexer at the receiver part to split these joint wavelengths apart.

After connecting the proposed wavelength router to the output of the proposed Panda ring resonator system, four generated wavelengths were used as optical sources. In order to compare superiority of the proposed solitonic system against the traditional WDM-based OWC systems, the same four wavelength lights were generated using CW lasers also. Rectangular and Gaussian pulse shapes were then generated with the same FSR and FWHM, and compared to the proposed solitonic pulse shape. The proposed system has been compared with traditional rectangular and Gaussian WDM-based OWC systems under equal conditions; the applied modulator is a non-return-to-zero 40 Gb/s pseudo random bit sequence of length 2^{31}-l, an equal input optical power of 30 mw, the same FSR of 3.7 ns and FWHM of 120 ps and the same AWGN OWC channel (range of 250 m, attenuation, geometrical loss, beam divergence, transmitter loss, additional losses and propagation delay).

In the Q-factor and BER analysis, OOK-NRZ modulation scheme is applied. There is a line of sight between the transmitter and receiver and the channel is not affected by path loss and multipath dispersion. The main source of noise is because of the background noise which is considered as a white Gaussian and the noises that affect the receiver are negligible. The transmitter filter converts the input bits to a train of pulses. Then the generated pulse train is multiplied by $2P_r$ and R, where P_r is the average power of the received optical signal and R is Photodetector responsivity. The channel is modelled as an AWGN channel which adds a noise n(t) to the propagating pulse. At the receiver, the received signal i(t) passes through the matched filter r(t), which is designed based on the generated pulse shape at the transmitter. Finally, a sampler and threshold detector determine the output.

The Q-factor of all the channels for a given 30 mw input power, are shown in Table 2. Higher Q-factor indicates a lower rate of energy loss. As can be seen from the table, the proposed solitonic method shows a considerably higher Q-factor and all the channels have a Q-factor of almost six or higher.

Table 2. Q-factor values for all the channels for a given 30 mw input power

Channel	Rectangular	Gaussian	Solitonic
0	4.90	5.38	6.01
1	4.53	5.21	5.92
2	5.76	6.35	6.70
3	5.02	5.87	6.39

Fig. 5 shows BER of the channel 4 for given input powers of 12 to 40 mw. As can be seen from Fig. 5, the proposed solitonic WDM-based OWC shows a lower BER compared to the traditional rectangular and Gaussian systems.

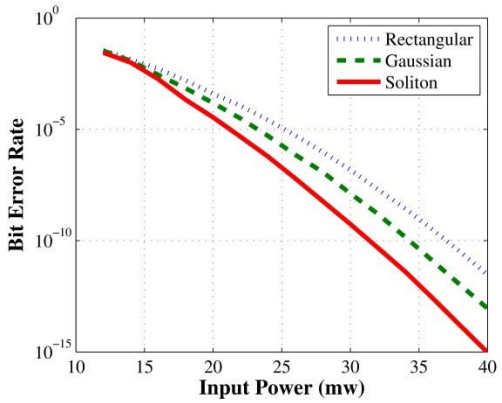

Fig. 5. BER against input power for different WDM-based OWC systems in an equal condition

For an input power of 30 mw, the proposed system achieves a BER of 4.2e-9 for channel 3 while the obtained results of BER for the traditional Gaussian and rectangular methods are 6.2e-7 and 8.6e-5, respectively. Therefore, the proposed system exhibits a greater robustness to adverse conditions and has the best performance in WDM-based OWC compared to the traditional rectangular and Gaussian methods. Consequently, the proposed method shows a better performance in dense and high speed WDM-based OWC applications compared to the traditional methods.

4. Conclusions

A system of Panda ring resonator connected to a wavelength router has been demonstrated. We have shown that WDM-based OWC reliability can be increased by the proposed system. With an optical Gaussian pulse input to the nonlinear Panda device, highly chaotic pulses were generated at the output with a wavelength router used to filter the dense wavelengths. The advantage of the system is that the proposed system can be integrated with the existing OWC transmitter and generated solitonic pulses, which show a better performance compared to other pulse shapes. Moreover, more and accurate soliton channels can be generated by using the proposed system. Using the obtained accurate channels and solitonic pulse, a faster WDM-based OWC with more channels is possible. As future work, we analyze WDM-based OWC system with more channels using the proposed method to increase the bitrate.

References

[1] S. Jovkova, M. Kavehard, Communications, IEEE Transactions **48**(6), 970 (2000).
[2] D.-Y. Song, Y.-S. Hurh, J.-W. Cho, J.-H. Lim, D.-W. Lee, J.-S. Lee, Y. Chung, Optics Express **7**(8), 280 (2000).
[3] M. C. Jeong, J. S. Lee, S. Y. Kim, S. W. Namgung, J. H. Lee, M. Y. Cho, S. W. Huh, Photonics Technology Letters **15**(1), 171 (2003).
[4] P. L. Chen, S. T. Chang, S. T. Ji, S. C. Lin, H. H. Lin, H. L. Tsay, P. H. Huang, W. C. Chiang, W. C. Lin, S. L. Lee, 2008 Digest of the IEEE/LEOS Summer Topical Meetingd 235 (2008).
[5] M. Matsumoto, K. Kazaura, P. Dat, A. Shah, K. Omae, T. Suzuki, K. Wakamori, T. Higashino, K. Tsukamoto, S. Komaki, Innovations in NGN: Future Network and Services, First ITU-T Kaleidoscope Academic Conference on, 221 (2008).
[6] K. Tsukamoto, T. Higashino, T. Nakamura, K. Takahashi, Y. Aburakawa, S. Komaki, K. Wakamori, T. Suzuki, K. Kazaura, A. M. Shah, PIERS Online **4**(1), 96 (2008).
[7] Y. Arimoto, M. Presi, V. Guarino, A. D'Errico, Optical Communication, 34th European Conference on, 1 (2008)
[8] E. Ciaramella, Y. Arimoto, G. Contestabile, M. Presi, A. D'Errico, V. Guarino, M. Matsumoto, Selected Areas in Communications, IEEE Journal, **27**(9), 1639 (2009).
[9] J. Libich, M. Komanec, S. Zvanovec, P. Pesek, W. O. Popoola, Z. Ghassemlooy, Optics Letters **40**(3), 391 (2015).
[10] J. Bohata, M. Komanec, J. Spáčil, Z. Ghassemlooy, S. Zvánovec, R. Slavík, Optics Letters **43**(5), 1035 (2018).
[11] R. Mata-Calvo, D. B. Calia, R. Barrios, M. Centrone, D. Giggenbach, G. Lombardi, P. Becker, I. Zayer, SPIE LASE Conference 12 (2017).
[12] V. Balaji, M. Murugan, S. Robinson, J. Optoelectron. Adv. M. **18**(11-12), 943 (2016).
[13] A. Shahidinejad, S. Soltanmohammadi, T. Anwar, Journal of Theoretical and Applied Information Technology **51**(2), 211 (2013).
[14] H. Moradi, H. Refai, P. LoPresti, Optoelectronics IET **6**(1), 34 (2012).
[15] X. Wang, X. Feng, P. Zhang, T. Wang, S. Gao, Optics Communications **387**, 43 (2017).
[16] K. O. Odeyemi, P. A. Owolawi, V. M. Srivastava, Optics Communications **382**, 205 (2017).
[17] X. Tang, Z. Xu, Z. Ghassemlooy, Journal of Lightwave Technology **31**(20), 3221 (2013).
[18] J. M. G. Balsells, M. Castillo-Vazquez, A. B. Moreno-Garrido, A. Puerta-Notario, Chinese Optics Letters **10**(4), 040101 (2012).
[19] I. S. Amiri, S. E. Alavi, M. R. K. Soltanian, R. Penny, Optical and Quantum Electronics **48**(1), 5 (2015).
[20] I. S. Amiri, M. N. Hindia, A. W. Reza, H. Ahmad, P. Yupapin, Optical Switching and Networking **25**, 13 (2017).
[21] S. E. Alavi, I. S. Amiri, S. M. Idrus, A. S. M. Supa'at, J. Ali, P. P. Yupapin, IEEE Photonics Journal, **6**(1), 1 (2014).
[22] I. S. Amiri, S. E. Alavi, S. M. Idrus, A. Nikoukar, J. Ali, IEEE Photonics Journal, **5**(5), 7901912 (2013).
[23] I. S. Amiri, J. Ali, P. P. Yupapin, International Journal of Modern Physics B **26**(4), 1 (2012).
[24] A. Shahidinejad, A. Azarpira, T. Anwar, O. Spaniol, J. Optoelectron. Adv. M. **16**(7-8), 892 (2014).

*Corresponding author: a.shahidinejad@gmail.com